



Supplement of

Aqueous-phase chemistry of glyoxal with multifunctional reduced nitrogen compounds: a potential missing route for secondary brown carbon

Yuemeng Ji et al.

Correspondence to: Taicheng An (antc99@gdut.edu.cn)

The copyright of individual parts of the supplement might differ from the article licence.

Supplement

S1 Experiments:

S1.1 Chemicals and Reagents

The chemicals purchased from Sigma Aldrich are as followings: glyoxal (GL, 40 wt% solution), ammonium sulfate (AS, > 99%), monoethanolamine (MEA, > 99%), Sulfuric acid (> 98%) and sodium hydroxide (> 96%) were purchased from Guangzhou Chemical Reagent Factory (Guangzhou, China). High-purity deionized water (18.2 M Ω cm) (Millipore Corp., USA) were used for dissolution and dilution.

S1.2 Mass spectrometry and chromatographic conditions

The selected chromatographic column was Hypersil GOLD C18 (100 \times 2.1 mm, 1.9 μ m). The injection volume was 1 μ L and the eluents were ultrapure water (eluent A) and acetonitrile (eluent B). The flow rate of mobile phase was 0.25 mL min⁻¹ with a gradient described as follows: First, starting with 2% B for 2 min, increasing to 95% B at 15 min, isocratic elution for 3 min, then decreasing to 2% B in 0.1 min and finally maintain 2% B to 20 min. Mass spectrometry detectors were equipped with a HESI source and set under the parameters as listed followingly: 4 kV spray voltage, 30 units of sheath gas flow, 10 units of auxiliary gas flow, 320 $^{\circ}$ C capillary temperature and 350 $^{\circ}$ C auxiliary gas heater temperature. MS mode was set with a scan range of 50-750 m/z with a resolution of 70000. While in MS² mode, the resolution was 17500.

S1.3 Detailed description of rate constants

The rate constant (k) with the ΔG^{\ddagger} value was calculated using Conventional Transition State theory (TST) (Eyring, 1935; Galano and Alvarez-Idaboy, 2009; Gao et al., 2014; Ji et al., 2022) as follows:

$$k_t = \sigma \frac{k_B T}{h} \exp\left(\frac{-\Delta G^{\ddagger}}{RT}\right) \quad (\text{S1})$$

where k_B and h are the Boltzmann and Planck constants, respectively; ΔG^{\ddagger} represents the activation energy of the reaction with the thermodynamic contribution corrections and solvent cage effects taken into consideration, and σ represents the reaction path degeneracy.

To simulate realistic conditions in the solution, the solvent cage effect, which was proposed by Okuno (Okuno, 1997), is incorporated into the free volume theory. Gibbs free energy is corrected by the

expression as follows:

$$\Delta G_{\text{sol}}^{\text{FV}} \cong \Delta G_{\text{sol}}^0 - RT\{\ln[n10^{(2n-2)}] - (n-1)\} \quad (\text{S2})$$

where ΔG_{sol}^0 is the Gibbs free energy of the reaction in the solution and n denotes the molecule number of the reaction. According to expression (2), the cage effects in the solution cause a decrease in the Gibbs free energy by 2.54 kcal mol⁻¹ for bimolecular reactions occurring at 298.15 K.

Thus, the apparent rate constant (k) obtained from the diffusion-limit effect (Collins and Kimball, 1949) can be calculated by the formula as follows:

$$k = \frac{k_t k_d}{k_t + k_d} \quad (\text{S3})$$

where the k_t is the thermal rate constant from expression (1). The diffusion-limited rate constant (k_d) for a bimolecular reaction is calculated as follows:

$$k_D = 4\pi R D_{AB} N_A \quad (\text{S4})$$

where R is the reaction distance, N_A denotes the Avogadro number; and D_{AB} is the mutual diffusion coefficient of the reactants A and B, which is the sum of diffusion coefficients of reactants A and B (D_A and D_B), i.e., $D_{AB} = D_A + D_B$ (Truhlar, 1985). D_A and D_B are estimated from the Stokes–Einstein approach (Einstein, 1905) listed in expression (5):

$$D = \frac{k_B T}{6\pi\eta\alpha} \quad (\text{S5})$$

where k_B is the Boltzmann constant, T is the temperature, η denotes the viscosity of the solvent, which is water in our case ($\eta = 8.9 \times 10^{-4}$ Pa s), and α is the radius of the solute.

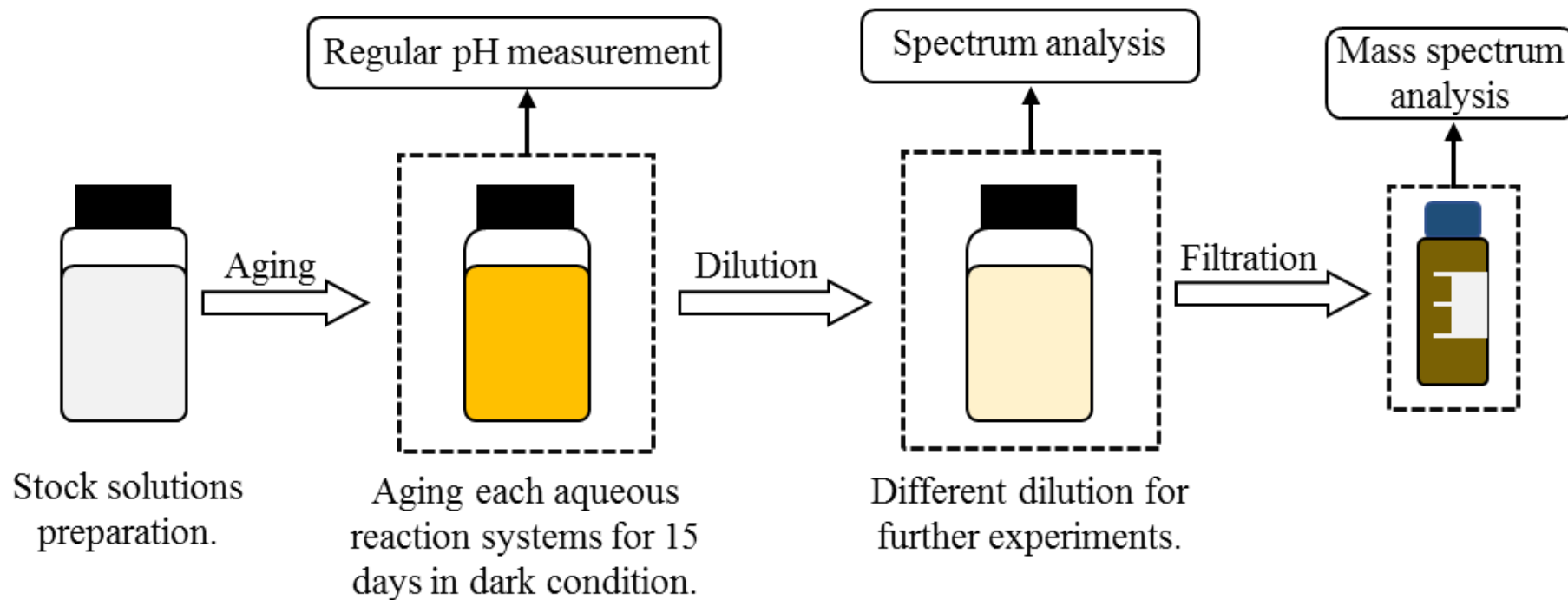


Figure S1. Experimental procedures.

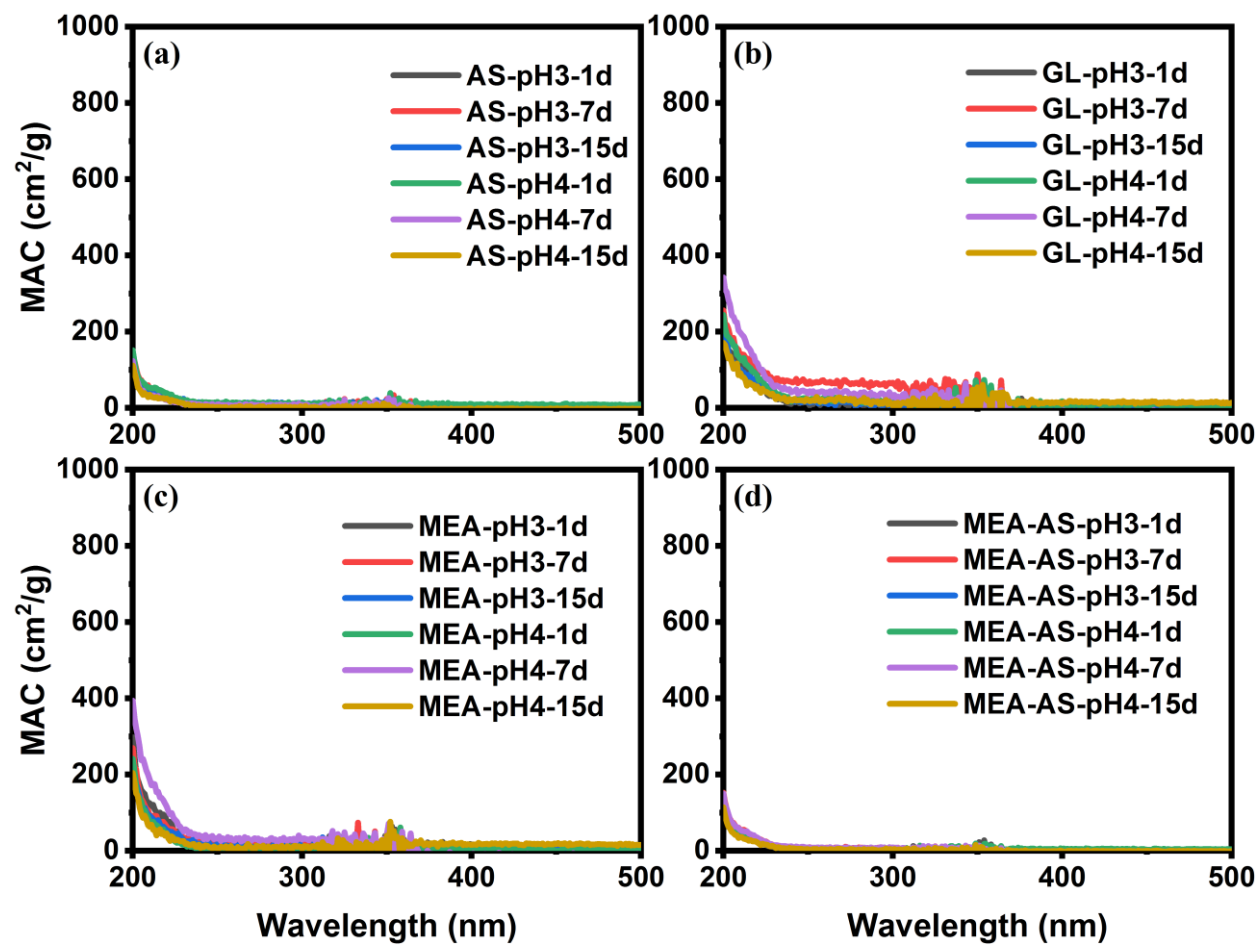


Figure S2. The MAC values of 1M (a) AS, (b) GL, (c) MEA and (d) MEA-AS solutions placed in dark over a time scale of 15 d.

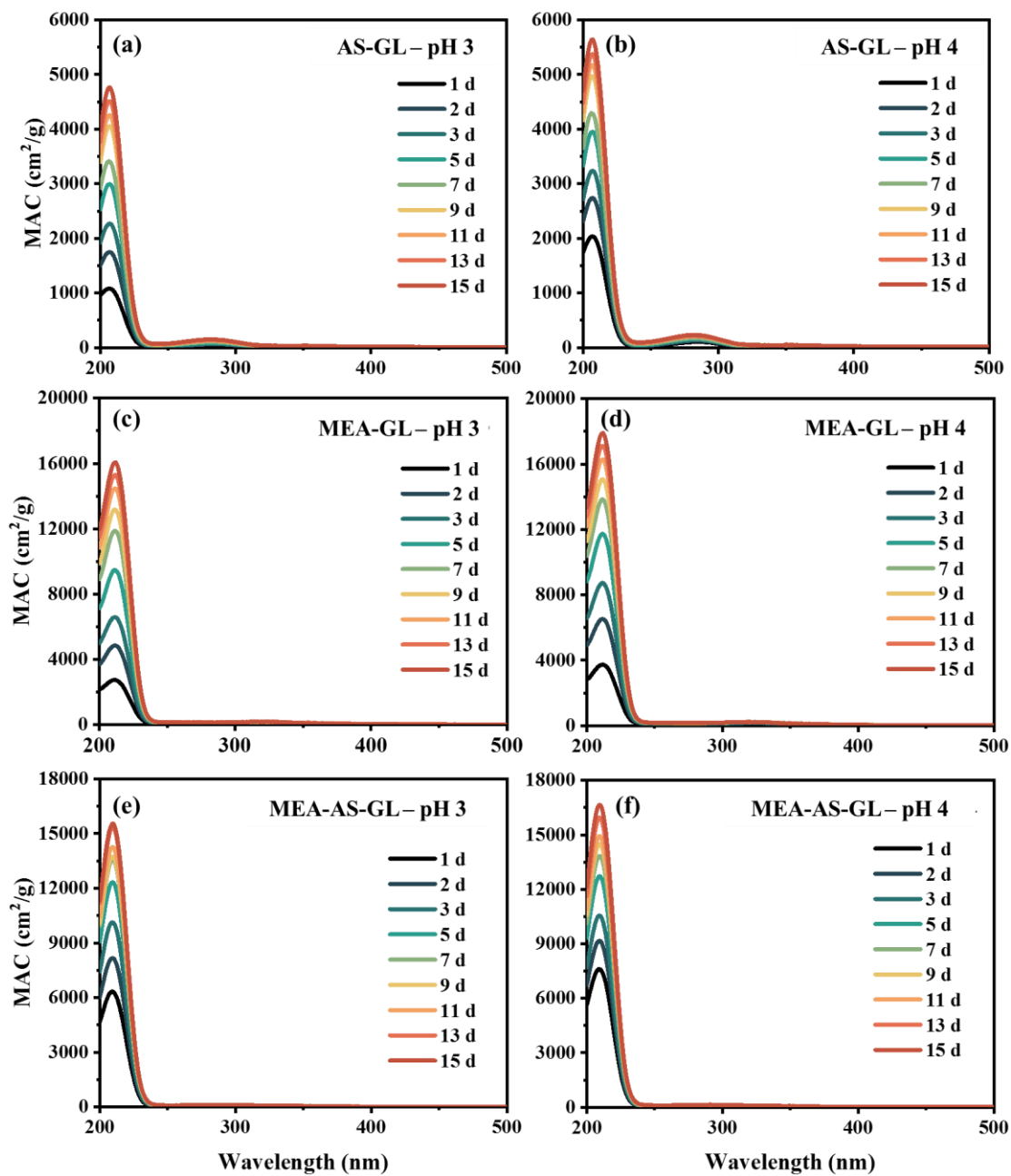


Figure S3. The MAC values for AS-GL (a and b), MEA-GL (c and d) and MEA-AS-GL (e and f) mixtures at the initial pH of 3 and 4 over a time scale of 15 d.

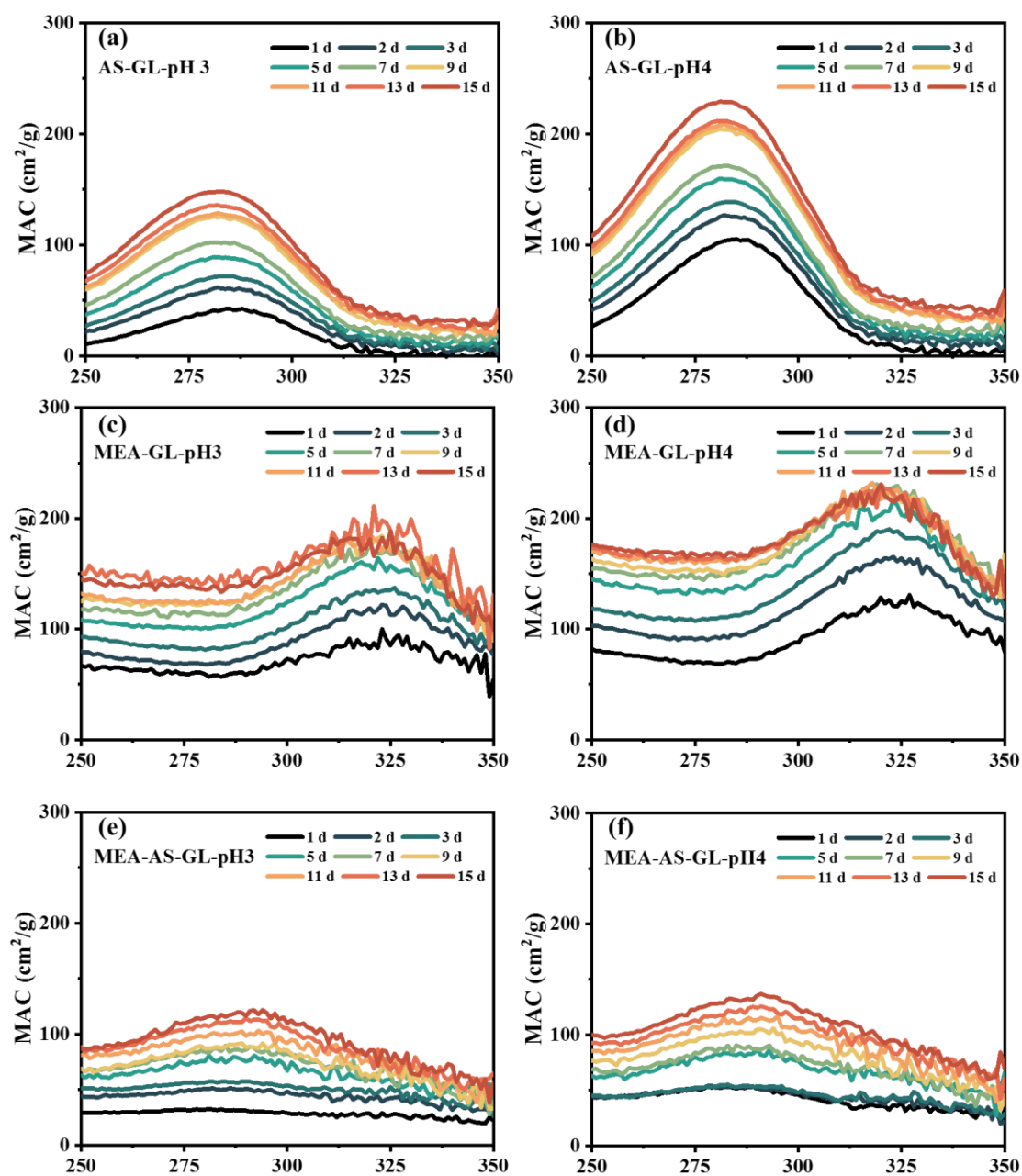


Figure S4. The MAC values for AS-GL (a and b), MEA-GL (c and d) and MEA-AS-GL (e and f) mixtures at the initial pH of 3 and 4 in the wavelength range of 250 - 350nm over a time scale of 15 d.

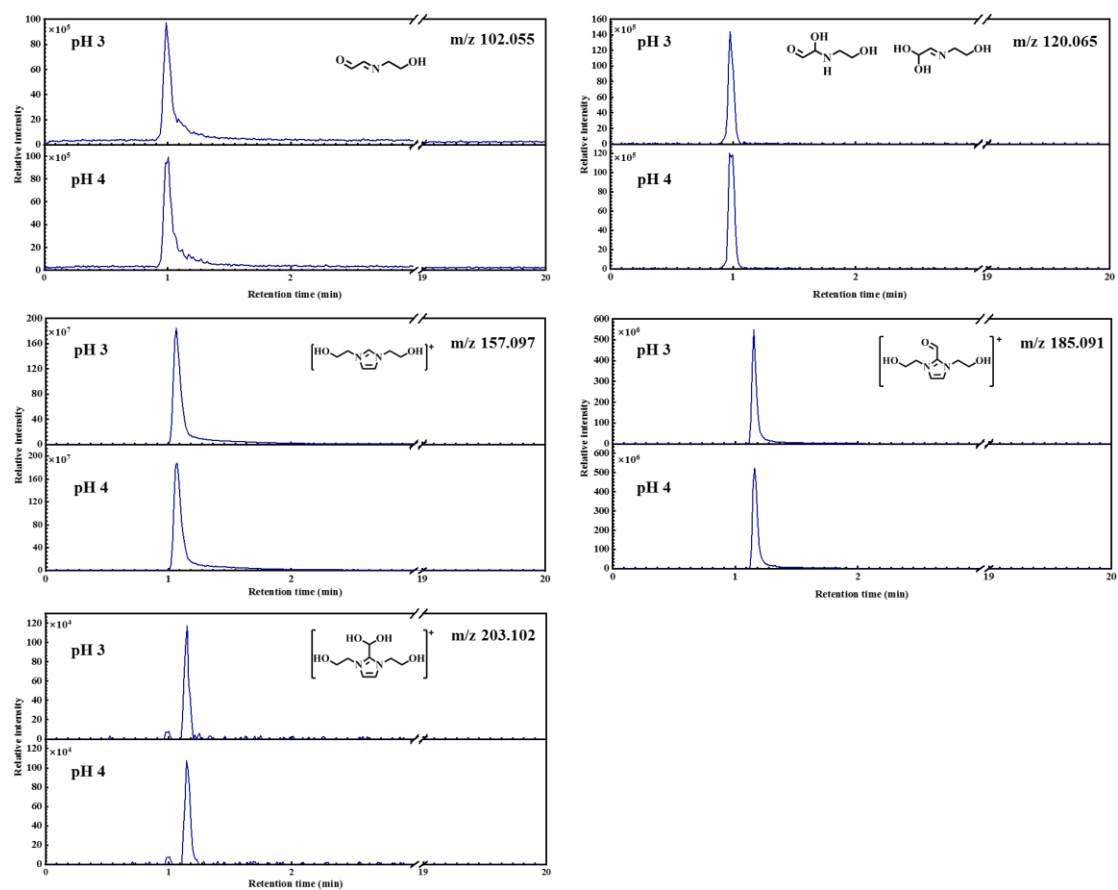


Figure S5. The extracted ion chromatograms of all reaction products for MEA-GL mixture at the initial pH of 3 and 4.

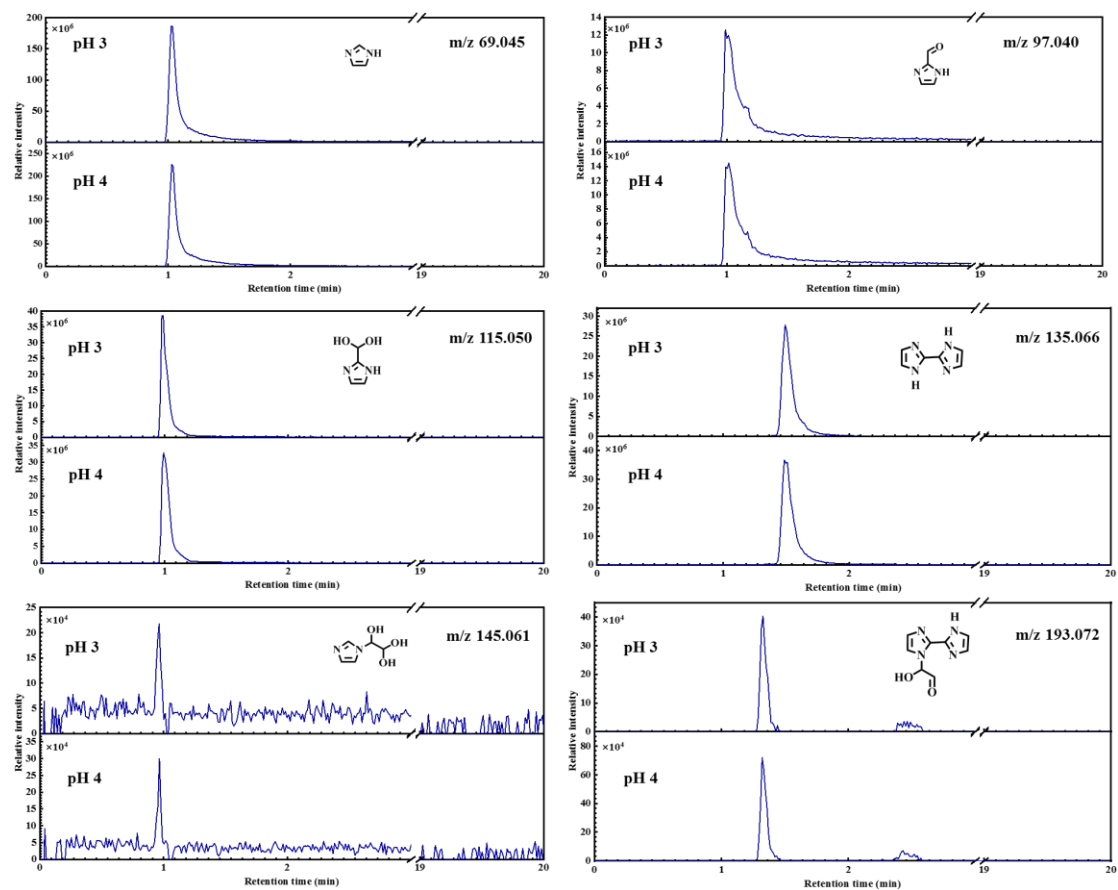


Figure S6. The extracted ion chromatograms of all reaction products for AS-GL mixture at the initial pH of 3 and 4.

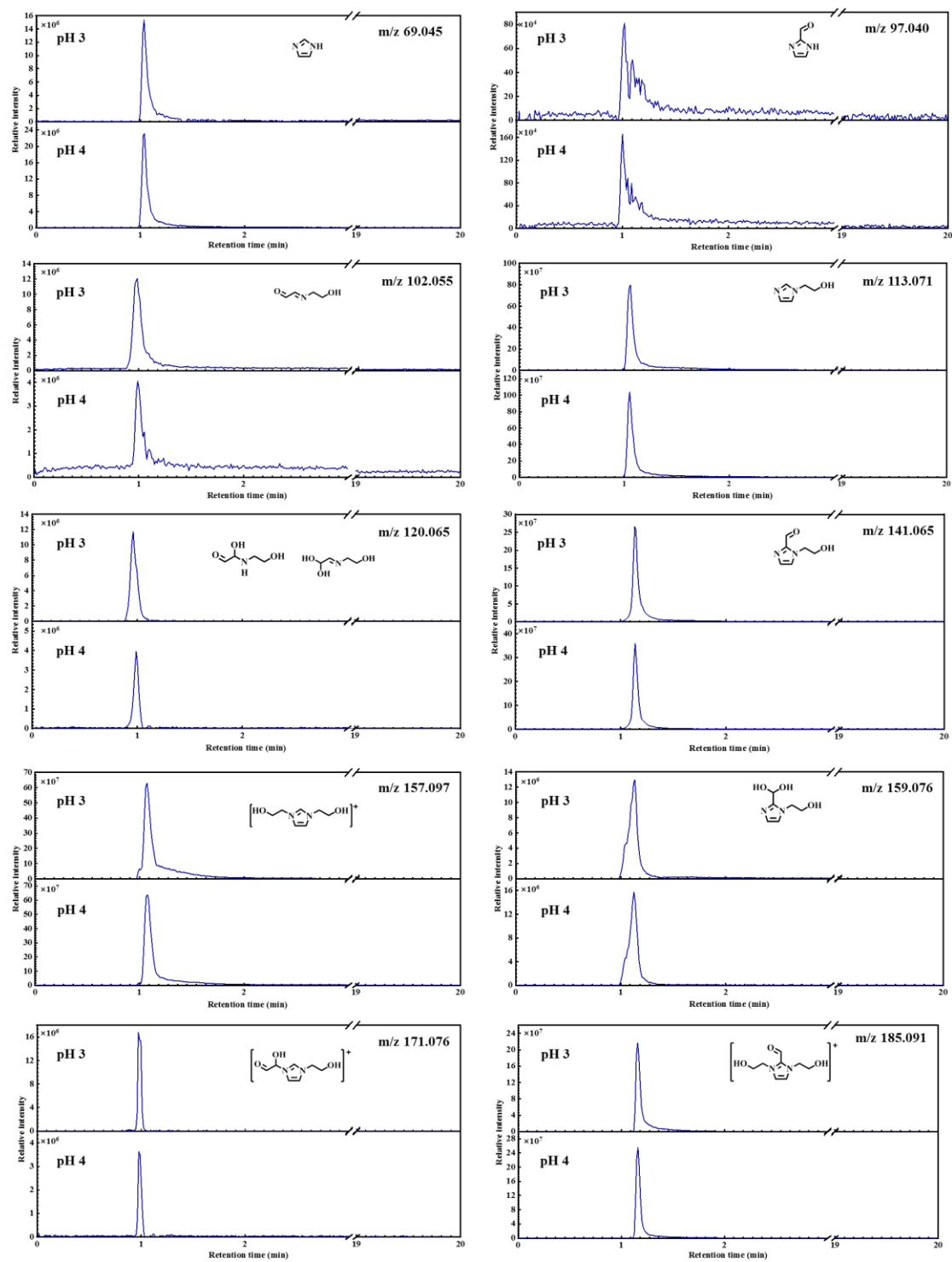


Figure S7. The extracted ion chromatograms of all reaction products for AS-MEA-GL mixture at the initial pH of 3 and 4.

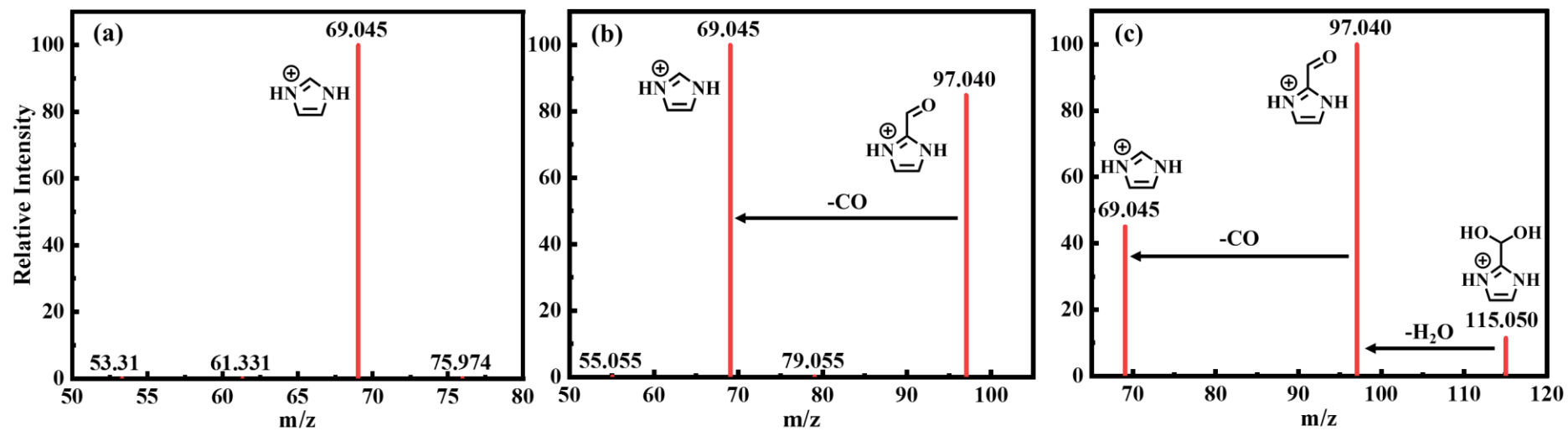


Figure S8. MS² spectra for m/z (a) 69.045, (b) 97.040 and (c) 115.050 with parent ions and fragments labeled on peaks (red). A few fragments with low intensity are removed.

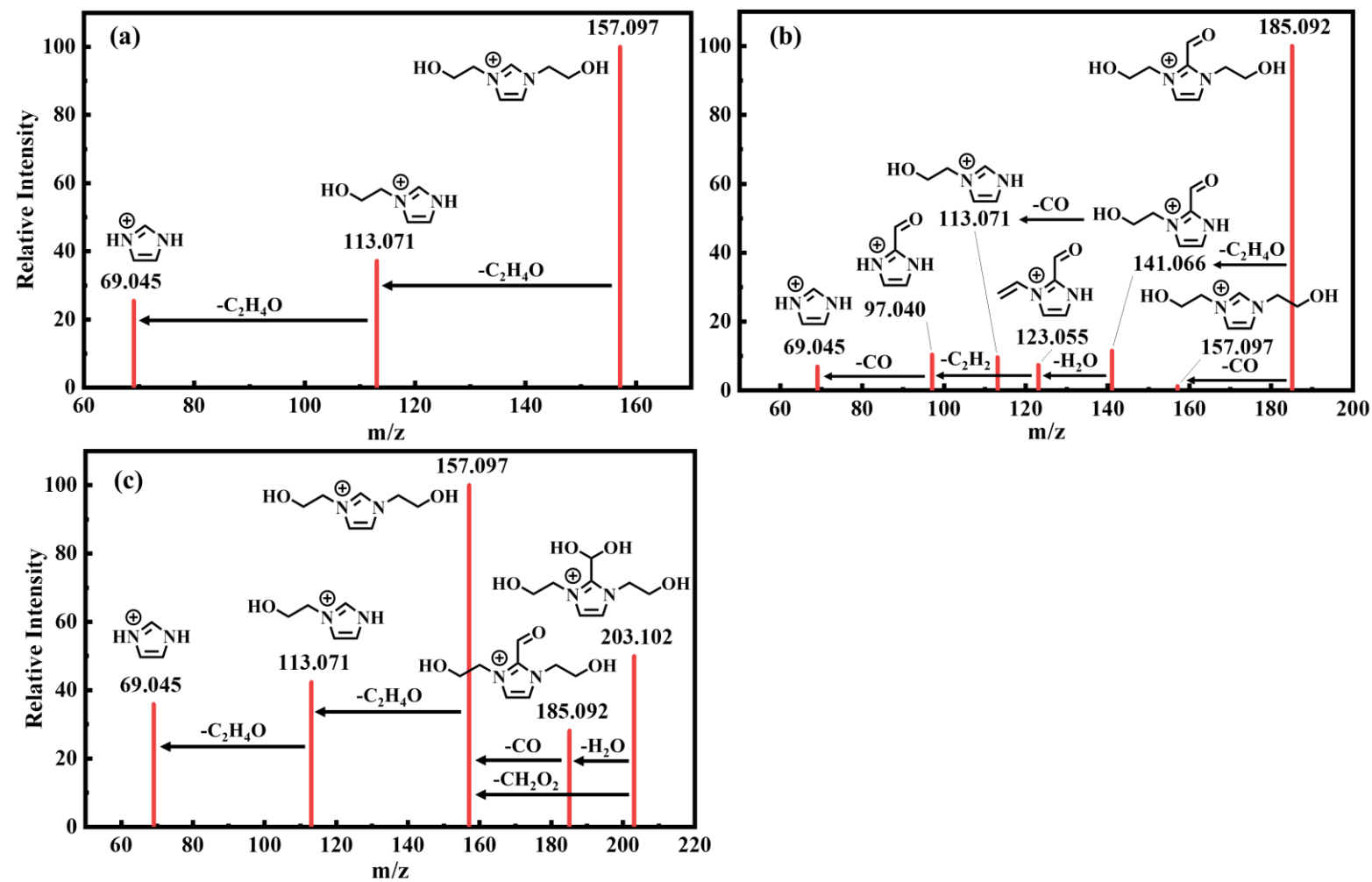


Figure S9. MS² spectra for m/z (a) 157.097, (b) 185.092 and (c) 203.102 with parent ions and fragments labeled on peaks (red). A few fragments with low intensity are removed.

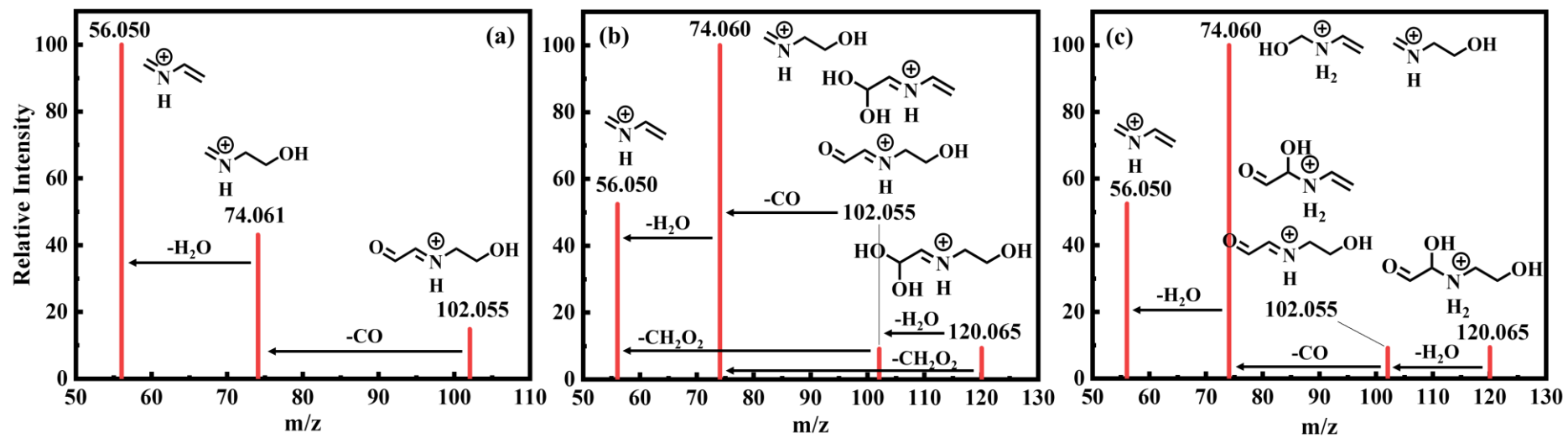


Figure S10. MS² spectrums for m/z (a) 102.055, (b) 120.065 and (c) its isomer with parent ions and fragments labeled on peaks (red). A few fragments with low intensity are removed.

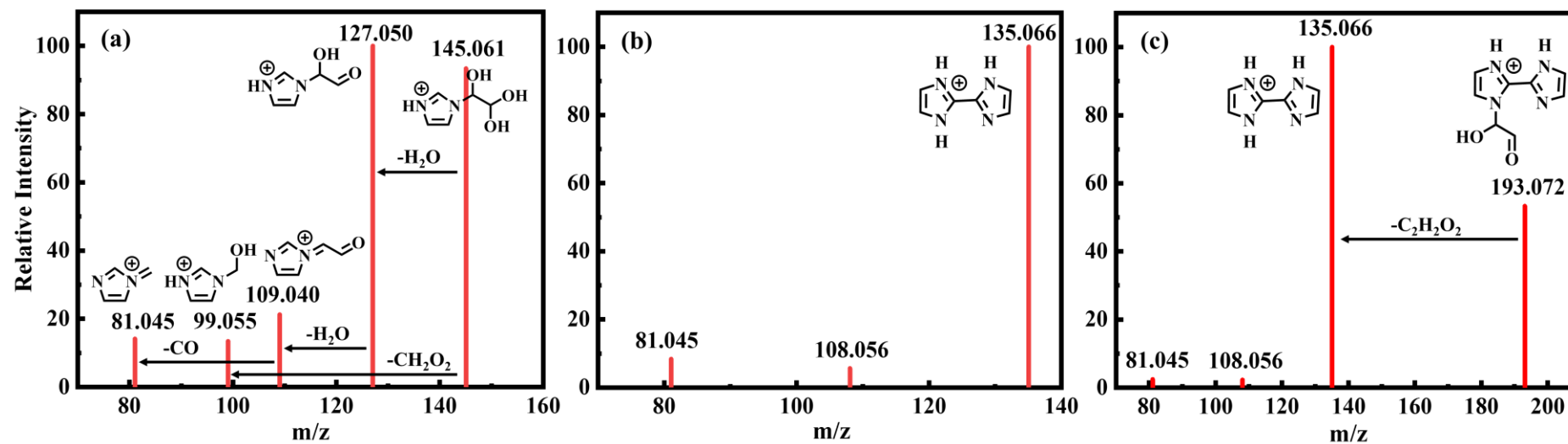


Figure S11. MS² spectrums for m/z (a) 145.061, (b) 135.066 and (c) 193.072 with parent ions and fragments labeled on peaks (red). A few fragments with low intensity are removed.

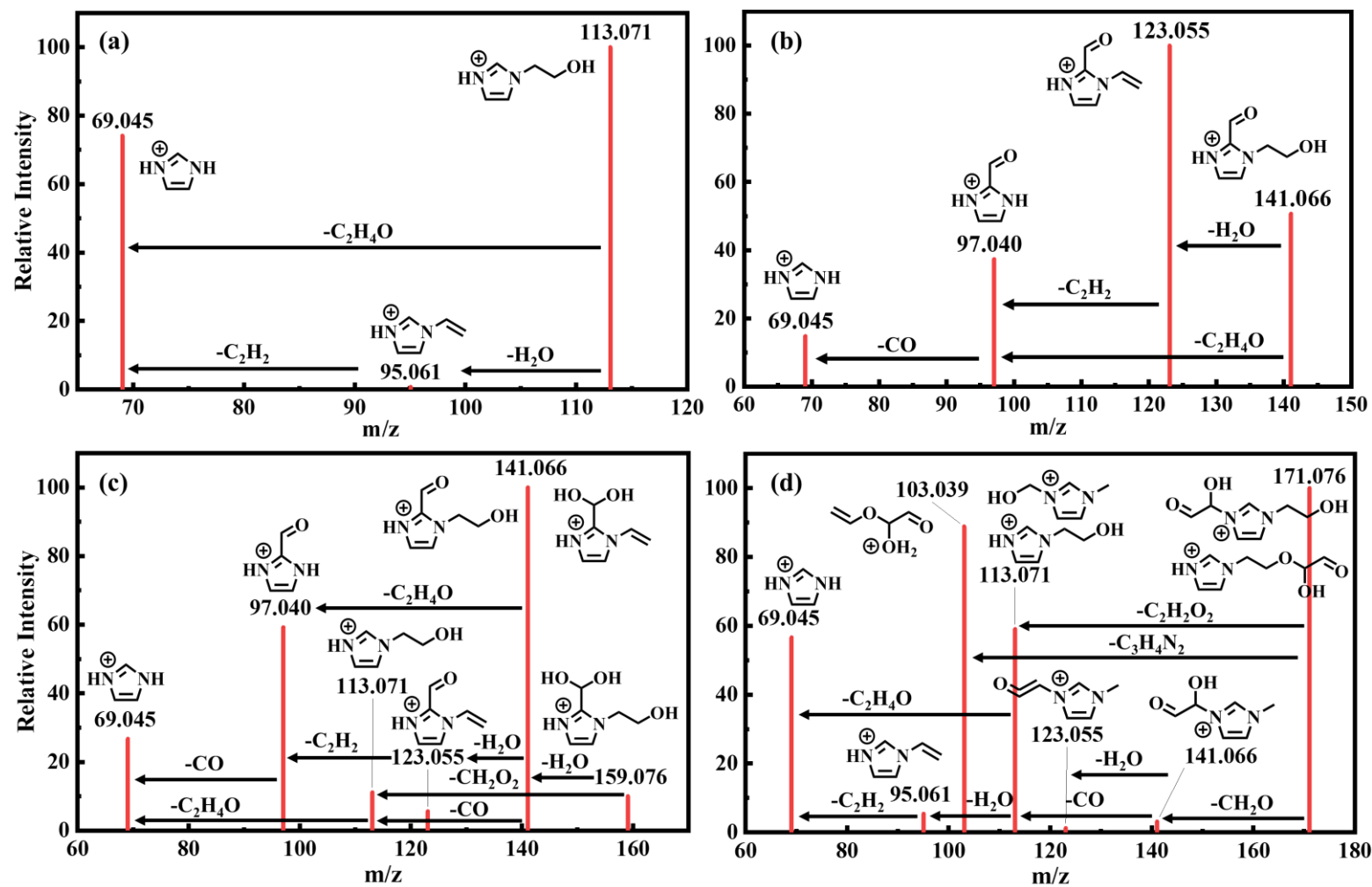


Figure S12. MS² spectrums for m/z (a) 113.071, (b) 141.066, (c) 159.076 and (d) 171.076 with parent ions and fragments labeled on peaks (red). A few fragments with low intensity are removed.

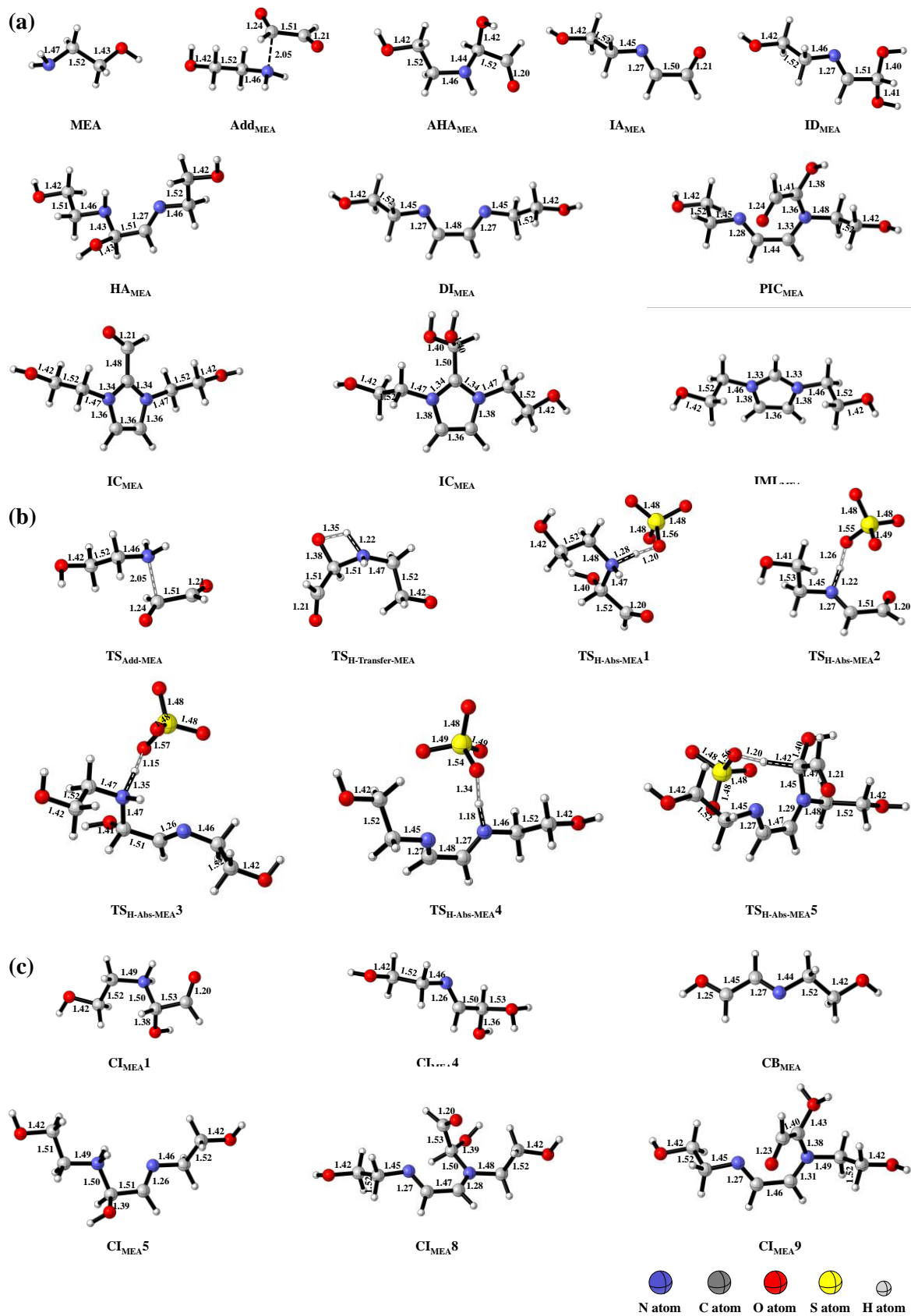


Figure S13. The optimized geometries of SPs including products (a), TSs (b) and CIs(c) in MEA-GL mixture. The structures were visualized by CYLview 1.0b software (Cylview).

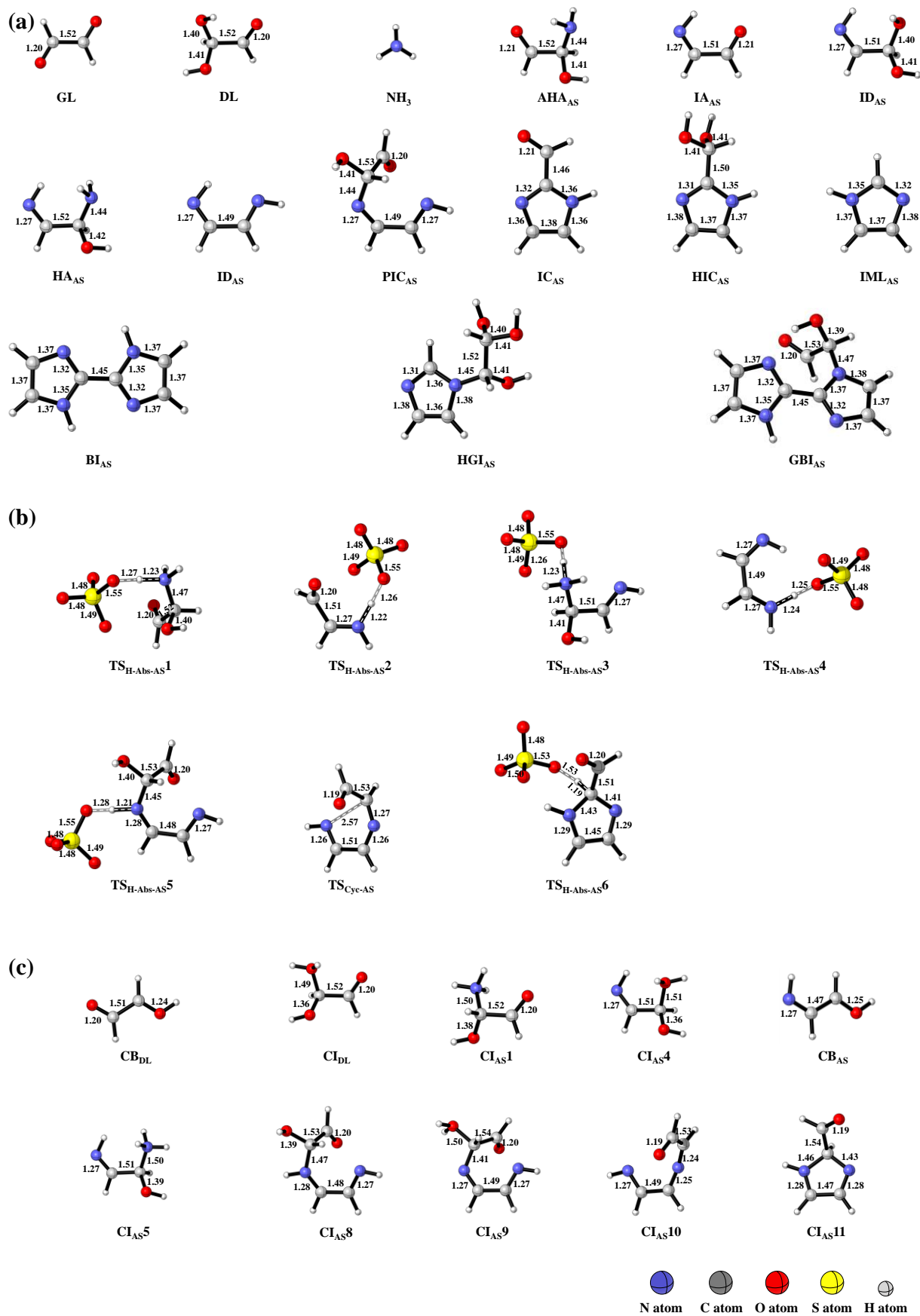


Figure S14. The optimized geometries of SPs including products (a), TSs (b) and CIs(c) in AS-GL mixture.

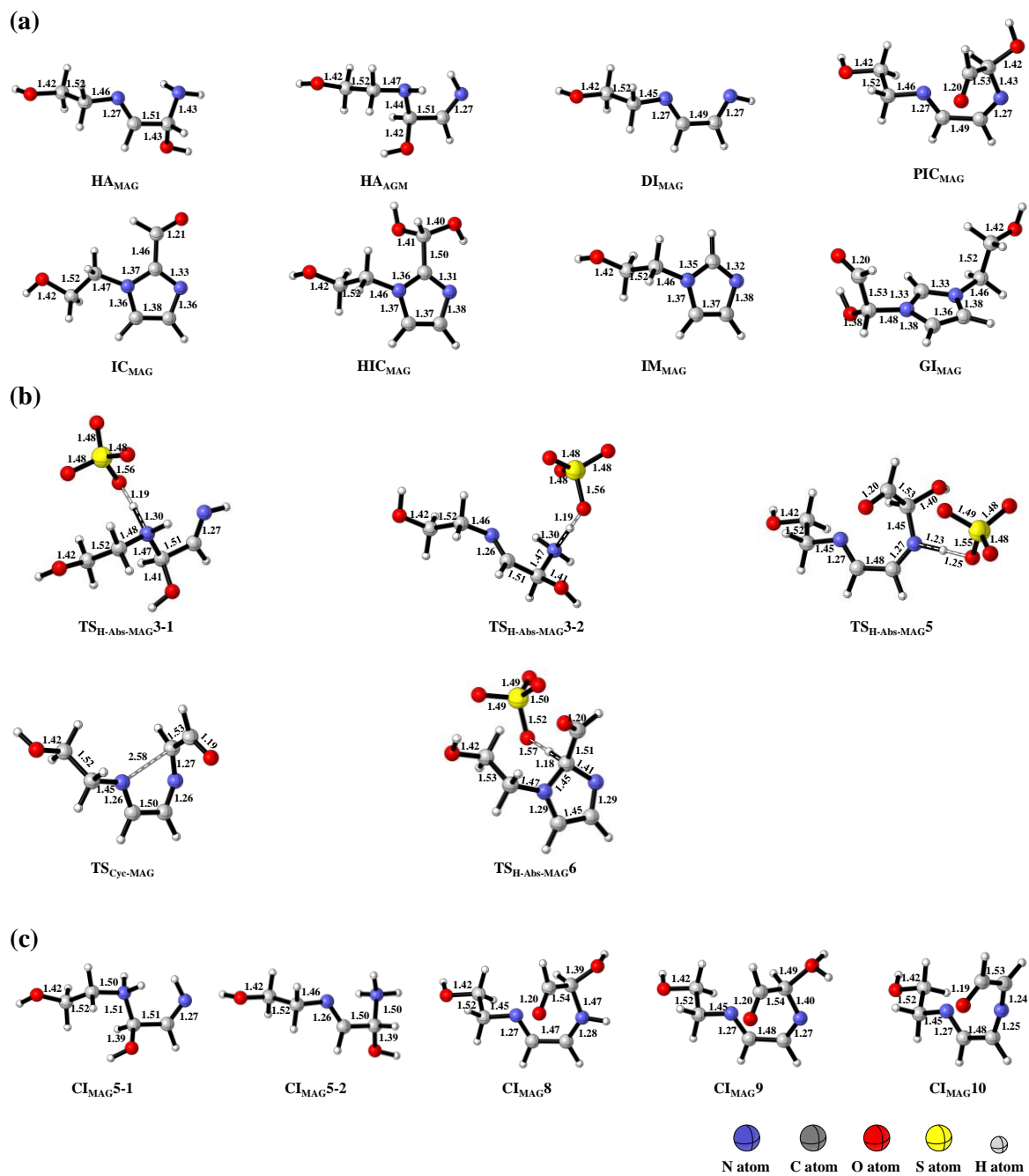


Figure S15. The optimized geometries of SPs including products (a), TSs (b) and CIs(c) in MEA-AS-GL mixture.

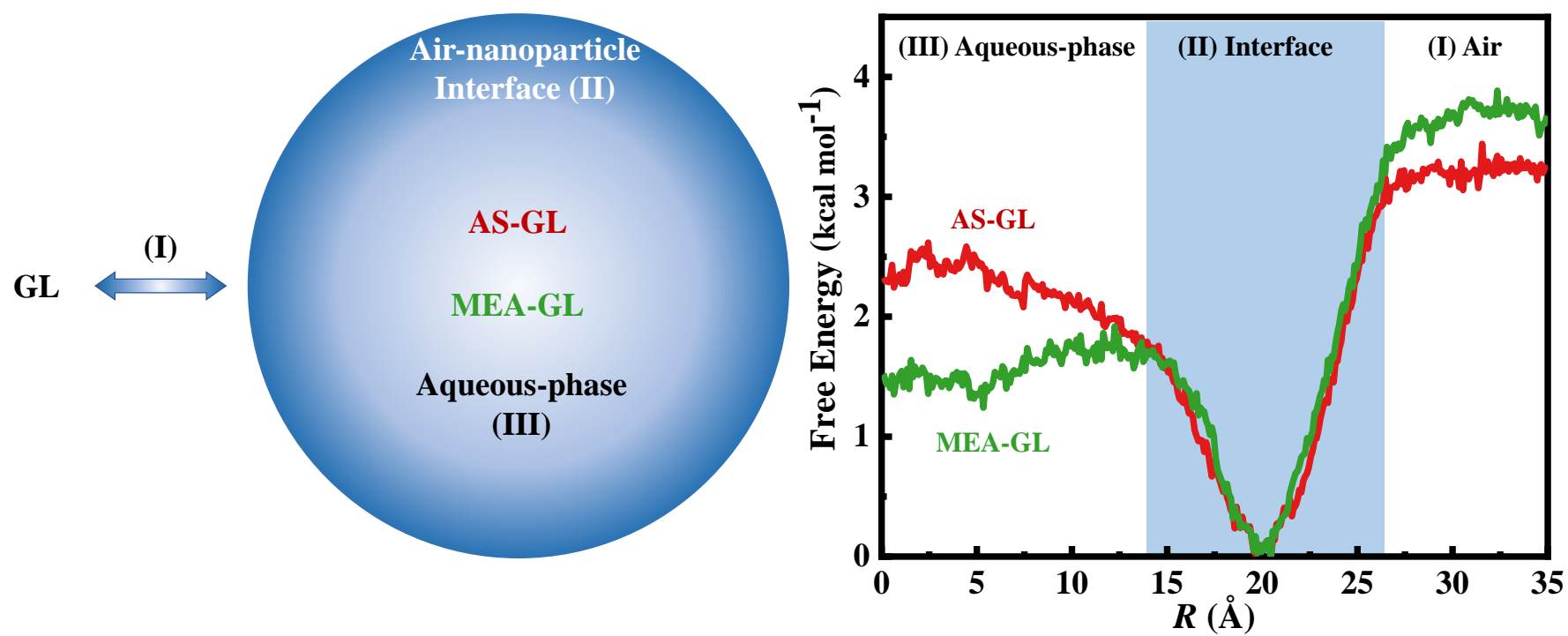

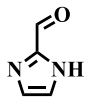
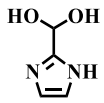
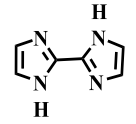
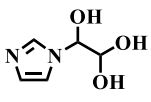
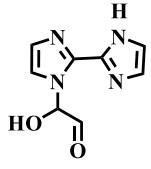
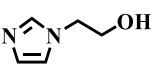
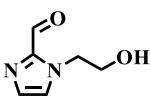
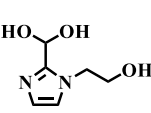
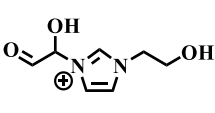
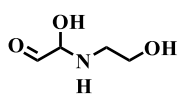
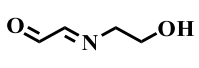
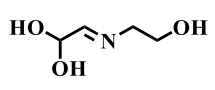

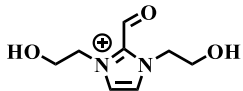
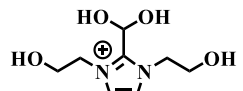


Figure S16. The critical processes of gaseous GL coming into the particles (left) and the free energy profile of gaseous GL approaching the MEA (green line) particle and AS (red line) particle (right).

Table S1. Structures and corresponding formulas, measured m/z values and fragments of products generated in MEA-GL, AS-GL and MEA-AS-GL mixtures.

Formulas	Measured m/z values (+ H ⁺)	Fragments (+ H ⁺)	Structures	Mixture	Name
C ₃ H ₄ N ₂	69.045	-		AS-GL MEA-AS-GL	IML _{AS}
C ₄ H ₄ N ₂ O	97.040	69.045		AS-GL MEA-AS-GL	IC _{AS}
C ₄ H ₆ N ₂ O ₂	115.050	97.040 69.045		AS-GL	HIC _{AS}
C ₆ H ₆ N ₄	135.067	81.045 108.056		AS-GL	BI _{AS}
C ₅ H ₈ N ₂ O ₃	145.060	127.050 109.040 81.045		AS-GL	HGI _{AS}
C ₈ H ₈ N ₄ O ₂	193.072	135.066 81.045		AS-GL	GBI _{AS}
C ₅ H ₈ N ₂ O	113.071	69.045 95.061		MEA-AS-GL	IML _{MAG}
C ₆ H ₈ N ₂ O ₂	141.066	123.055 97.040 69.045		MEA-AS-GL	IC _{MAG}
C ₆ H ₁₀ N ₂ O ₃	159.076	141.066 97.040 69.045		MEA-AS-GL	HIC _{MAG}
C ₇ H ₁₁ N ₂ O ₃	171.076	103.039 113.071 69.045		MEA-AS-GL	GI _{MAG}
C ₄ H ₉ NO ₃	120.066	74.061 56.050 102.055		MEA-GL MEA-AS-GL	AH _{AMEA}
C ₄ H ₇ NO ₂	102.055	56.050 74.060		MEA-GL MEA-AS-GL	IA _{MEA}
C ₄ H ₉ NO ₃	120.066	74.060 56.050 102.055		MEA-GL MEA-AS-GL	ID _{MEA}

Formulas	Measured m/z values (+ H ⁺)	Fragments (+ H ⁺)	Structures	Mixture	Name
C ₇ H ₁₃ N ₂ O ₂	157.097	113.071 69.045		MEA-GL MEA-AS-GL	IML _{MEA}
C ₈ H ₁₃ N ₂ O ₃	185.092	141.065 97.040 113.071		MEA-GL MEA-AS-GL	IC _{MEA}
C ₈ H ₁₅ N ₂ O ₄	203.102	157.097 113.071 69.045		MEA-GL	HIC _{MEA}

*The fragments are ordered by intensity in descending and the ones with the most abundant intensity are written in bold.

Table S2. Average pH values of all reaction systems with initial pH 3 or 4 over a time scale of 15 d.

Reaction	AS-GL	AS-GL	MEA-GL	MEA-GL	MEA-AS-GL	MEA-AS-GL
Time (d)	(pH3)	(pH4)	(pH3)	(pH4)	(pH3)	(pH4)
Initial pH	3.01	4.02	3.01	3.97	3.03	3.99
1	2.55	2.64	2.22	2.32	1.81	1.93
2	2.39	2.46	2.00	1.98	1.71	1.81
3	2.31	2.37	1.85	1.87	1.62	1.75
5	2.21	2.26	1.69	1.67	1.51	1.65
7	2.15	2.20	1.59	1.65	/	1.60
9	2.09	2.14	1.52	1.55	1.56	1.59
11	2.07	2.12	1.55	1.56	1.54	1.53
13	2.03	2.08	1.50	1.55	1.52	1.53
15	2.03	2.07	1.47	1.48	1.49	1.55

Table S3. The activation barrier energies (ΔG^\ddagger), the reaction energy (ΔG_r), and the rate constants (k) for the protonation pathways from N-containing CIs. Herein, the units of energies and rate constants are kcal mol⁻¹ and M⁻¹ s⁻¹, respectively.

Reactions	ΔG^\ddagger	ΔG_r	k
MEA-GL mixture:			
GL + MEA \rightarrow Add _{MEA}	6.3	6.4	2.68×10^8
Add _{MEA} \rightarrow AHA _{MEA}	15.2	-13.9	^b 38
CI _{MEA1} + SO ₄ ²⁻ \rightarrow AHA _{MEA} + HSO ₄ ⁻	-4.5	-7.7	1.27×10^9
CI _{MEA5} + SO ₄ ²⁻ \rightarrow HA _{MEA} + HSO ₄ ⁻	-2.3	-5.3	1.16×10^9
CI _{MEA8} + SO ₄ ²⁻ \rightarrow PIC _{MEA} + HSO ₄ ⁻	17.5	-0.2	1.74
AS-GL mixture:			
GL + NH ₃ \rightarrow Add _{AS}	8.6	5.8	5.78×10^6
Add _{AS} \rightarrow AHA _{AS}	18.2	-11.9	^b 2.48×10^{-1}
CI _{AS1} + SO ₄ ²⁻ \rightarrow AHA _{AS} + HSO ₄ ⁻	-3.4	-7.0	1.41×10^9
CI _{AS5} + SO ₄ ²⁻ \rightarrow HA _{AS} + HSO ₄ ⁻	-5.3	-7.5	1.40×10^9
CI _{AS8} + SO ₄ ²⁻ \rightarrow PIC _{AS} + HSO ₄ ⁻	-5.0	-12.4	1.34×10^9
CI _{AS10} \rightarrow CI _{AS11}	3.9	-33.5	^a 3.03×10^{10} ^b 8.35×10^9
CI _{AS11} + SO ₄ ²⁻ \rightarrow IC _{AS} + HSO ₄ ⁻	-0.6	-42.5	1.59×10^9
MEA-AS-GL mixture:			
CI _{MAG5-1} + SO ₄ ²⁻ \rightarrow HA _{AGM} + HSO ₄ ⁻	-6.7	-8.3	1.23×10^9
CI _{MAG5-2} + SO ₄ ²⁻ \rightarrow HA _{MAG} + HSO ₄ ⁻	-0.8	-4.4	1.23×10^9
CI _{MAG8} + SO ₄ ²⁻ \rightarrow PIC _{MAG} + HSO ₄ ⁻	-5.4	-11.3	1.26×10^9
CI _{MAG10} \rightarrow CI _{MAG11}	5.0	-32.8	^a 4.15×10^9 ^b 1.29×10^9
CI _{MAG11} + SO ₄ ²⁻ \rightarrow IC _{MAG} + HSO ₄ ⁻	1.6	-39.4	1.61×10^9

Calculated via ^aKisthelp or ^bscript.

References

- Collins, F. C. and Kimball, G. E.: Diffusion-controlled reaction rates, *J. Colloid Sci.*, 4, 425-437, [https://doi.org/10.1016/0095-8522\(49\)90023-9](https://doi.org/10.1016/0095-8522(49)90023-9), 1949.
- CYLview, b. L., C. Y., Université de Sherbrooke, 2009 (<http://www.cylview.org>): [code],
- Einstein, A.: Über die von der molekularkinetischen Theorie der Wärme geforderte Bewegung von in ruhenden Flüssigkeiten suspendierten Teilchen, *Ann. Phys.*, 322, 549-560, <https://doi.org/10.1002/andp.19053220806>, 1905.
- Eyring, H.: The Activated Complex in Chemical Reactions, *J. Chem. Phys.*, 3, 107-115, <https://doi.org/10.1063/1.1749604>, 1935.
- Galano, A. and Alvarez-Idaboy, J. R.: Guanosine + OH Radical Reaction in Aqueous Solution: A Reinterpretation of the UV-vis Data Based on Thermodynamic and Kinetic Calculations, *Org. Lett.*, 11, 5114-5117, <https://doi.org/10.1021/ol901862h>, 2009.
- Gao, Y., Ji, Y., Li, G., and An, T.: Mechanism, kinetics and toxicity assessment of OH-initiated transformation of triclosan in aquatic environments, *Water Res.*, 49, 360-370, <https://doi.org/10.1016/j.watres.2013.10.027>, 2014.
- Ji, Y., Shi, Q., Ma, X., Gao, L., Wang, J., Li, Y., Gao, Y., Li, G., Zhang, R., and An, T.: Elucidating the critical oligomeric steps in secondary organic aerosol and brown carbon formation, *Atmos. Chem. Phys.*, 22, 7259-7271, <https://doi.org/10.5194/acp-22-7259-2022>, 2022.
- Okuno, Y.: Theoretical Investigation of the Mechanism of the Baeyer-Villiger Reaction in Nonpolar Solvents, *Chem. - Eur. J.*, 3, 212-218, <https://doi.org/10.1002/chem.19970030208>, 1997.
- Truhlar, D. G.: Nearly encounter-controlled reactions: The equivalence of the steady-state and diffusional viewpoints, *J. Chem. Educ.*, 62, 104, <https://doi.org/10.1021/ed062p104>, 1985.